Molecular Pharmacology Fast Forward. Published on June 21, 2013 as doi: 10.1124/mol.113.087080
This article has not been copyedited and formatted. The final version may differ from this version.

MOL #87080

Title Page

Hits of a High-Throughput Screen Identify the Hydrophobic Pocket of Autotaxin/Lysophospholipase D as an Inhibitory Surface

James I. Fells, Sue Chin Lee, Yuko Fujiwara, Derek D. Norman, Keng Gat Lim, Ryoko Tsukahara, Jianxiong Liu, Renukadevi Patil, Duane D. Miller, R. Jason Kirby, Sandra Nelson, William Seibel, Ruben Papoian, Abby L. Parrill, Daniel L. Baker, Robert Bittman and Gabor Tigyi

Dept. of Physiology, University of Tennessee Health Science Center, Memphis, TN(JF, SCL, YF, DN, KGL, RT, JL, GT)

Dept. of Pharmaceutical Sciences, University of Tennessee Health Science Center, Memphis, TN (RP, DM)

Drug Discovery Center, University of Cincinnati, Cincinnati, OH, (RK, SN, WS, RP)

Computational Research on Materials Institute, Department of Chemistry, University of Memphis, Memphis, TN(AP, DB)

Department of Chemistry and Biochemistry, Queens College of The City University of New York, Flushing, New York (RB)

Molecular Pharmacology Fast Forward. Published on June 21, 2013 as DOI: 10.1124/mol.113.087080
This article has not been copyedited and formatted. The final version may differ from this version.

Running Title Page

Running title: Novel inhibitory surface in autotaxin

Corresponding Author:

Gabor Tigyi, M.D., Ph.D.
Department of Physiology, UTHSC
894 Union Avenue
Memphis TN 38163
Tel.: 901-448-4793
Fax: 901-448-7126
Email: gtigyi@uthsc.edu

Document statistics:

Number of text pages: 32
Number of tables: 4
Number of figures: 6
Number of references: 50
Number of words in the Abstract: 250
Number of words in Introduction: 810
Number of words in Discussion: 1347
Supplemental material online: 1

List of non-standard abbreviations:

ADMANLPC, analog 3-acyl-7-dimethylaminonaphthyl - 1-LPC; ATCC, American Type Culture Collection, ATX, autotaxin; compound ***1***, 2,4-dichloro-N-(3-fluorophenyl)-5-(4-morpholinylsulfonyl) benzamide; compound ***2***, 4-Oxo-4-{2-[(5-phenoxy-1H-indol-2-yl)carbonyl]hydrazino}x-N-(4-phenylbutan-2-yl)butanamide;compound ***3***, N-(2,6-dimethylphenyl)-2-[N-(2-furylmethyl)(4-(1,2,3,4-tetraazolyl)phenyl)carbonylamino]-2-(4-hydroxy-3-methoxyphenyl) acetamide; DMEM, Dulbecco's modified Eagle's medium; DMSO, dimethyl sulfoxide; FS-3, fluorogenic substrate 3; GPCR,G-protein coupled receptors; HA155, Z)-4-((4-((3-(4-Fluorobenzyl)-2,4-dioxo-1,3-thiazolan-5-yliden)-methyl)phenoxy)methyl)benzeneboronic acid ATX Inhibitor IV; HEK293T, human embryonic kidney cell line 293T; HTS, high-throughput screening; LPA, lysophosphatidic acid; LPAR, LPA receptor; LPC, lysophosphatidylcholine; LPL, lysophospholipase; NPP, nucleotide pyrophosphatase/phosphodiesterase; PDSP, Psychoactive Drug Screening Program; PBS, phosphate buffered saline; PDE, phosphodiesterase; PEG, polyethylene glycol; pNP-TMP, *p*-nitrophenyl thymidine 5'-monophosphate; S1P, sphingosine 1-phosphate; UC-DDC, University of Cincinnati Drug Discovery Center (http://www.drugdiscovery.uc.edu/).

Molecular Pharmacology Fast Forward. Published on June 21, 2013 as DOI: 10.1124/mol.113.087080
This article has not been copyedited and formatted. The final version may differ from this version.

Abstract

The lysophospholipase D (autotaxin, ATX) plays an important role in cancer invasion, metastasis, tumor progression, tumorigenesis, neuropathic pain, fibrotic diseases, cholestatic pruritus, lymphocyte homing, and thrombotic diseases by producing the lipid mediator lysophosphatidic acid (LPA). A high-throughput screen of ATX inhibition using the lysophosphatidylcholine (LPC) -like substrate fluorogenic substrate 3 (FS-3) and ~10,000 compounds from the University of Cincinnati Drug Discovery Center (UC DDC) identified several small-molecule inhibitors with IC_{50} values ranging from nanomolar to low micromolar. The pharmacology of the three most potent compounds, 918013 (***1***), 931126 (***2***), and 966791 (***3***) were further characterized in enzyme, cellular, and whole animal models. Compounds ***1*** and ***2*** were competitive inhibitors of ATX-mediated hydrolysis of the lysophospholipase substrate FS-3. In contrast, compound ***3*** was a competitive inhibitor of both FS-3 and the phosphodiesterase substrate *p*-nitrophenyl thymidine 5'-monophosphate. Computational docking and mutagenesis suggested that compounds ***1*** and ***2*** target the hydrophobic pocket thereby blocking access to the active site of ATX. The potencies of compounds ***1-3*** were comparable to each other in each of the assays. All of these compounds significantly reduced invasion of A2058 human melanoma cells *in vitro* and the colonization of lung metastases by B16-F10 murine melanoma cells in C57BL/6 mice. The compounds had no agonist or antagonist effects on select lysophosphatidic acid (LPA) and S1P receptors, nor did they inhibit nucleotide pyrophosphatase /phosphodiesterase (NPP) enzymes NPP6 and NPP7. These results identify the molecular surface of the hydrophobic pocket of ATX as a target-binding site for inhibitors of enzymatic activity.

Molecular Pharmacology Fast Forward. Published on June 21, 2013 as DOI: 10.1124/mol.113.087080
This article has not been copyedited and formatted. The final version may differ from this version.

Introduction

Autotaxin (ATX, NPP2) is member of the nucleotide pyrophosphatase /phosphodiesterase (NPP) family of enzymes that was originally discovered as a secreted factor that promoted the invasion and motility of melanoma cells (Stracke et al., 1992). The dual lysophospholipase (LPL) and phosphodiesterase (PDE) activity of ATX is catalyzed by the same active site (Gijsbers et al., 2003). While hydrolysis of nucleotide pyrophosphates does not appear to be physiologically relevant *in vivo* (Baker et al., 2006; Clair et al., 2003; Koh et al., 2003), hydrolysis of lysophosphatidylcholine (LPC), which is considered to be the physiologically relevant substrate of ATX, generates the bioactive lipid lysophosphatidic acid (LPA). A variety of biological processes are mediated by LPA via activation of multiple G-protein coupled receptors (GPCRs) (Tigyi, 2010; Yanagida et al., 2013). Some of these responses—including angiogenesis, chemotaxis, cell invasion, migration, proliferation, and suppression of apoptosis—are particularly important in tumor biology because they affect the growth, progression, and metastasis of many types of cancers (Brindley et al., 2013; Houben and Moolenaar, 2011; Mills and Moolenaar, 2003). Upregulated ATX expression has been reported in numerous cancers including thyroid, prostate, breast, and ovarian cancers, as well as melanoma (David et al., 2010; Kehlen et al., 2004; Nouh et al., 2009; Wu et al., 2010; Yang et al., 2002; Yang et al., 1999). In addition to malignant diseases, ATX has been implicated in neuropathic pain, fibrotic diseases, cholestatic pruritus, lymphocyte homing, chronic inflammatory conditions, and thrombotic diseases (Ikeda and Yatomi, 2012; Kremer et al., 2012; Moolenaar et al., 2013; Nikitopoulou et al., 2012; Tager, 2012; Ueda et al., 2013). Because of the established role of LPA in

these malignancies, inhibition of ATX represents a therapeutically attractive target for the disruption of the ATX-LPA-LPA receptor (LPAR) signaling axis (Albers and Ovaa, 2012).

At the present time there is no approved ATX inhibitor available for therapy; however, development of ATX inhibitors has gained increasing interest with several small-molecule ATX inhibitors having been described (Albers et al., 2010; Ferry et al., 2008; Gierse et al., 2010; Gotoh et al., 2012; Hoeglund et al., 2010; Kawaguchi et al., 2013; Mize et al., 2011; Saunders et al., 2008; St-Coeur et al., 2013) A considerable amount of effort has been devoted to the characterization of these inhibitors that interact with the active site of ATX. Recent crystal structures of ATX, including a co-crystal with the irreversible inhibitor HA155(Hausmann et al., 2011), and the active-site inhibitor BoA set of compounds (Kawaguchi et al., 2013) have provided new insight into the catalytic site of this enzyme and also shed light on the access of the lipid substrate to the active site (Hausmann et al., 2011; Nishimasu et al., 2011). The structure reported by Nishimasu *et al*., shows LPA in a hydrophobic channel that suggests an exit route for the product connecting the catalytic site to the enzyme surface.

Our objective in the present study was to apply a new high-throughput screening (HTS) strategy with the synthetic LPC-like substrate FS-3 for novel ATX inhibitors using 10,000 compounds representative of the chemical diversity space of the ~360,000 compounds contained in the University of Cincinnati Drug Discovery Center (UC-DDC) chemical library. Previous HTS strategies targeting ATX (Albers et al., 2010; Ferry et al., 2008) used the nucleotide-like PDE substrate *p*-nitrophenyl thymidine 5'-monophosphate (pNP-TMP). In our strategy, hits that inhibited ATX activity by 50% at a concentration of

Molecular Pharmacology Fast Forward. Published on June 21, 2013 as DOI: 10.1124/mol.113.087080
This article has not been copyedited and formatted. The final version may differ from this version.

10 μM were selected for further characterization using pNP-TMP and another LPC analog 3-acyl-7-dimethylaminonaphtyl - 1-LPC (ADMAN-LPC). Using these LPL and PDE substrates our hits fell into two categories (Figure 1): The first category of compounds, exemplified by 2,4-dichloro-N-(3-fluorophenyl)-5-(4-morpholinylsulfonyl) benzamide (UC-DDC number 918013, designated as compound ***1***) and 4-oxo-4-{2-[(5-phenoxy-1H-indol-2-yl)carbonyl]hydrazino}-N-(4-phenylbutan-2-yl)butanamide (UC-DDC number 931126, designated as compound ***2***) are competitive inhibitors of the hydrolysis of LPC-type substrates only (termed herein as single inhibitors).

A second category of compounds, represented by compound N-(2,6-dimethylphenyl)-2-[N-(2-furylmethyl)(4-(1,2,3,4-tetraazolyl)phenyl)carbonylamino]-2-(4-hydroxy-3-methoxyphenyl) acetamide (UC-DDC number 966791, designated as compound ***3***), competitively inhibited the hydrolysis of both types of substrates via a competitive mechanism(termed herein as dual-inhibitor). Computational docking of compounds ***1*** and ***2*** into the ATX crystal structure suggests that they interact with a surface in the hydrophobic pocket of ATX. In contrast, compound ***3*** interacts with a surface at the catalytic site. Alanine replacement of residue Phe^{275} in the hydrophobic inhibitor-interacting surface reduced the inhibition of FS-3 hydrolysis by compound ***1***, whereas it had no effect on the action of the dual-inhibitor compound ***3***. The hydrolysis of pNP-TMP by the $F^{275}A$ mutant was also blocked by compound ***3***. All three compounds dose-dependently reduced the ATX-dependent invasion of A2058 melanoma cells *in vitro*. The single inhibitor compound ***1*** and the dual inhibitor compound ***3***, when administered to C57BL/6 mice inoculated with the B16 melanoma cells, reduced the number of metastatic lung nodules. These results identify the hydrophobic channel surface as a

Molecular Pharmacology Fast Forward. Published on June 21, 2013 as DOI: 10.1124/mol.113.087080
This article has not been copyedited and formatted. The final version may differ from this version.

novel inhibitory site in the ATX structure amenable to drug discovery.

Molecular Pharmacology Fast Forward. Published on June 21, 2013 as DOI: 10.1124/mol.113.087080
This article has not been copyedited and formatted. The final version may differ from this version.

Materials and Methods

Reagents. A ~10,000-member diversity library was provided by the UC DDC. Compounds ***1*** and ***3*** were also purchased from TimTec; and ChemBridge for the animal studies. The compounds were diluted in DMSO at a 10mM stock concentration at -80°C. PNP-TMP was purchased from Sigma-Aldrich, FS-3 was purchased from Echelon, while ADMAN-LPC was synthesized as previously described (Baker et al., 2006).

Expression, Purification, and Activity of ATX. The expression, purification, and enzymatic assay conditions of human ATX were described previously (Gupte et al., 2011).

Primary HTS assay conditions. Before the start of the assay, 20µL of 4nM ATX per well were dispensed into 384-well plates. The assay was started immediately by dispensing 10 µM of the test compounds in dimethyl sulfoxide (DMSO; final DMSO concentration, 0.093%), DMSO alone (0% inhibition control), or LPA (final concentration, 10 µM,100% inhibition control) to the appropriate wells. Next, 10 µL of 4 µM FS-3(1 µM final) in assay buffer (50 mM Tris, 1 mM $MgCl_2$, 1 mM $CaCl_2$, 3 mM KCl, 140 mM NaCl, 15 µM bovine serum albumin) was added to all wells. Plates were briefly centrifuged for 35 seconds at 337 x g. An initial fluorescence was read by fluorescence excitation at 475 nm and detection of emission at 535 nm using a Vision Plate reader. The plates were then incubated for 3 hours at 37°C. Autotaxin activity was determined after 3 hours by the change in fluorescence. Dose response curves were recorded to determine IC_{50} values for compounds that caused >50% inhibition of ATX enzyme activity.

Molecular Pharmacology Fast Forward. Published on June 21, 2013 as DOI: 10.1124/mol.113.087080
This article has not been copyedited and formatted. The final version may differ from this version.

Secondary assay conditions for inhibition of PDE activity using pNP-TMP substrate. The assay contained overall concentrations of 4 nM ATX, 1 mM pNP-TMP, and 10 µM of compound in assay buffer. Absorbance was monitored at 485 nm after 4 hours of incubation to measure enzyme activity.

Tertiary screen in the presence of 0.01% Triton X-100. A detergent-dependent screen was adapted from the previously described enzyme assay, for the identification of promiscuous inhibitors. Triton X-100 was added to assay buffer at a concentration of 0.01% to test interference with FS-3 and pNP-TMP hydrolysis assays.

Amplex Red Choline Release Assay. Inhibition of ATX-mediated hydrolysis of various chain-length LPC substrates was determined via Amplex Red choline release assay as described previously (Hoeglund et al., 2010; North et al., 2010). Briefly, 60 µl triplicate reaction volumes were loaded into 96-well, half-area plates (Corning Inc.) in assay buffer consisting of 50 mM Tris, 5 mM $CaCl_2$, 30 µM fatty acid-free BSA (pH 7.4). Final concentrations of reaction constituents were 0.1 U/ml choline oxidase (MP Biomedicals), 1 U/ml horseradish peroxidase (Thermo-Fisher Scientific), 10 µM Amplex Red (Life Technologies), 10 nM ATX, 100 µM LPC (14:0, 16:0, 18:0 or 18:1 chain lengths from Avanti Polar Lipids, Alabaster, AL) and 10 µM inhibitor. Fluorescence was measured at excitation and emission wavelengths of 560 and 590 nm, respectively, initially and after 2 hour incubation at 37°C. From the background-corrected endpoint data, percent ATX inhibition versus vehicle control was calculated for each triplicate data set and reported ± standard deviation.

Quaternary screen using ADMAN-LPC. ADMAN-LPC at a final concentration of 30 µM was resuspended in assay buffer containing 2 mg/ml BSA with or without 10 µM

Molecular Pharmacology Fast Forward. Published on June 21, 2013 as DOI: 10.1124/mol.113.087080
This article has not been copyedited and formatted. The final version may differ from this version.

inhibitor compound and 30 nM ATX. The reaction was incubated at 37 °C for 4 h. Lipids were extracted using a modification of the Bligh and Dyer procedure by adding 3.5 volumes of citrate phosphate buffer, pH 4, before addition of chloroform and methanol (2:1 v/v). Lipids were dried and resuspended in 30 µl chlorform/methanol (1:1) and separated on silica gel 60 TLC plates (Merck) using $CHCl_3$/MeOH/NH_4OH (60:35:8 v/v/v). Fluorescent LPC and LPA species were visualized by UV transillumination and quantified via densitometric analysis in the NIH ImageJ software ((Schneider et al., 2012)Schneider et al., 2012) in order to compare LPA production and ATX inhibition.

Determination of the Mechanism of Autotaxin Inhibition. The mechanism of ATX inhibition was determined using an activity assay with inhibitor concentrations of 0, 0.5, and 2 times the experimentally determined IC_{50} value and FS-3 substrate concentrations ranging from 0.3 to 20 µM. The initial reaction rate was determined by plotting background-corrected fluorescence at emission wavelength 485 nm as a function of time using 528 nm excitation of the fluorochrome. Data were then transformed using a carboxyfluorescein standard curve, which is analogous to the fluorescent FS-3 hydrolytic product. Reaction rate was then plotted as a function of FS-3 concentration and simultaneously fitted via non-linear regression using the Michaelis-Menten equations for competitive, non-competitive, uncompetitive, and mixed-mode inhibition as described in our previous publication Gupte et al. (Gupte et al., 2011) using GraphPad Prism v5 (GraphPad Software Inc.). The model providing the highest global non-linear fit (R^2) value, taking into account GraphPad's interpretation rules for the calculated α value, was selected as the mechanism of inhibition. K_i (compound affinity for enzyme) was subsequently calculated based on the corresponding regression

Molecular Pharmacology Fast Forward. Published on June 21, 2013 as DOI: 10.1124/mol.113.087080
This article has not been copyedited and formatted. The final version may differ from this version.

analysis.

Testing of off-target effects of select ATX inhibitors. Compounds ***1*** and ***3*** were submitted to PDSP (Psychoactive Drug Screening Program) for analysis of effect at 10 μM on 32 various human transporters and receptors.

Molecular docking of the inhibitors to the ATX crystal structure. All of the molecular docking studies were carried out using Autodock Vina.(Trott and Olson, 2010) The crystal structure of ATX (PDB ID: 2XRG) was chosen as the structure of reference protein.(Hausmann et al., 2011) All water molecules, sugars, iodoacetamide, and non-polar hydrogen atoms were removed; Zinc heteroatoms records were retained. The binding site was defined by centering the docking box around catalytic domain containing the co-crystallized inhibitor HA155. Both the enzyme and ligands were prepped using the Racoon software (Forli, 2013). Docking simulations were run using the default settings of this program.

Site-Directed Mutagenesis and Transfection. Amino-terminal FLAG epitope-tagged ATX constructs were subcloned into pcDNA3.1 vector (Invitrogen). Constructs were mutated using the QuikChange II XL site-directed mutagenesis kit (Stratagene). TOP10 competent cells (Invitrogen) were transformed with the mutant constructs, and clones were verified by complete sequencing of the inserts. Human embryonic kidney cells (HEK293T) were cultured in Dulbecco's modified Eagle's medium (DMEM) containing 10% heat inactivated fetal calf serum and 2 mM L-glutamine in a 10 cm dish. The cells were grown overnight at 37°C and 5% CO_2 up to 80% confluence before transfection. Transfection was done in the presence of Effectene® transfection reagent from Qiagen according to the manufacturer's protocol. Twenty hours post-transfection, the culture

Molecular Pharmacology Fast Forward. Published on June 21, 2013 as DOI: 10.1124/mol.113.087080
This article has not been copyedited and formatted. The final version may differ from this version.

medium was changed to serum-free DMEM. Forty-eight hours post-transfection, the conditioned serum-free medium containing secreted ATX mutants was collected and concentrated in ATX assay buffer using 10,000 molecular weight cutoff filters (Millipore) by centrifugation at 3000 × g.

Inhibition of ATX-dependent A2058 melanoma cell invasion. A2058 melanoma cells (gift from Dr. Timothy Clair, NCI, National Institutes of Health) were cultured in DMEM containing 10% (V/V) FBS, 2 mM L-glutamine, 100 U mL^{-1} penicillin, and 100 µg mL^{-1} streptomycin. Cell invasion across a matrigel-coated membrane was performed using the 24-well BD BioCoat^{TM} tumor invasion system (BD Biosciences, 8µm-pore size). 5 x 10^4 cells in serum-free DMEM supplemented with 0.1% BSA were added to the upper chamber. The chemoattractant (recombinant ATX plus 1µM of 18:1 LPC) was added in 0.75 ml of serum-free DMEM/0.1% BSA to the bottom chamber. Where indicated, the various compounds were pre-incubated in serum-free DMEM/0.1% BSA with recombinant ATX for 30 min at 37°C, prior to the addition of 1µM LPC and placed in the bottom chamber. Cells were left to invade the matrigel for 16 h at 37°C. After incubation, the medium in the upper chamber was removed and the insert was transferred into a new 24-well plate containing 4µg/ml of calcein AM (Molecular Probes, Invitrogen) in Hank's balanced salt solution (HBSS). The plates were incubated for 1 h at 37°C. The fluorescence of invaded cells was measured with a FLEXStation II plate reader (Molecular Devices) at excitation and emission wavelengths of 485 and 530nm, respectively.

Melanoma lung colonization model. All animal procedures were approved by the Institutional Animal Care and Use Committee at the University of Tennessee. Eight- to

Molecular Pharmacology Fast Forward. Published on June 21, 2013 as DOI: 10.1124/mol.113.087080
This article has not been copyedited and formatted. The final version may differ from this version.

twelve- week-old female C57Bl/6 mice (Charles River) were injected with 7.5 x 10^4 B16F10 cells in 100 µl conditioned medium via tail veins. The groups then received either compound ***1*****,** compound ***3*****,** or 4-pentadecylbenzylphosphonic acid, an ATX inhibitor we developed and validated earlier (Gupte et al., 2011) at 30 µg per mouse via intraperitoneal injection starting one day before or after the B16-F10 injection, and daily for an additional 10 days. Control mice were injected with vehicle (PBS with 10% PEG vehicle). Subsequently, animals were monitored for another 10 days without treatment. On day 21, all mice were sacrificed; the lungs were harvested, inflated, and fixed with 10% formalin. The number of metastatic nodules on the lung surface was counted. The number of lung nodules was compared against the vehicle-treated control group by Student's T test, and $p < 0.05$ was considered significant

Molecular Pharmacology Fast Forward. Published on June 21, 2013 as DOI: 10.1124/mol.113.087080
This article has not been copyedited and formatted. The final version may differ from this version.

Results

The primary objective of the present study was to experimentally identify a new and diverse set of non-lipid compounds that modulate the LPL activity of human recombinant ATX against the FS-3 substrate. To achieve this we developed a HTS method of ATX in 40 µL assay volume (Supplementary Figure 1). In this assay a 10 µM concentration of LPA, which acts as a feedback inhibitor of ATX, caused an average 85% inhibition of the catalytic activity after a 3 h incubation. The Z' value was 0.847 (range from 0.554 – 0.924) with a mean signal to background ratio of 4.19 (range 3.14 – 4.70) indicating the robustness of the assay. In order to maximize diversity, a chemical library of 9,652 compounds from the UC DDC library of 360,000 compounds was assembled and screened at 10 µM to identify novel compounds that inhibited ATX activation. A compound was defined as a hit if it showed >50% inhibition of FS-3 hydrolysis. From the primary screening, 198 inhibitory compounds (SupplementalTable 1) were selected (2% hit rate). Hits were further reduced by applying a series of filters, including a 10-point dose response for each confirmed hit. The average Z' value for the dose-response assay was 0.75, ranging from 0.57 to 0.83. Signal to background ratios [(+) ATX to (-) ATX] averaged 3.38 and ranged from 2.28 to 4.14. A compound was selected for further characterization if it had an $IC_{50} \leq 1\mu M$. Evaluation of the initial 198 compounds led to 26 compounds (SupplementalTable **2**) that were chosen for further screening.

Secondary, tertiary, and quaternary screening of the primary hits. The 26 compounds were subsequently screened against the PDE substrate pNP-TMP (Figures 2B and 3B). This screen revealed two groups of ATX inhibitors: 14 compounds that

Molecular Pharmacology Fast Forward. Published on June 21, 2013 as DOI: 10.1124/mol.113.087080
This article has not been copyedited and formatted. The final version may differ from this version.

inhibited FS-3 hydrolysis only and 12 compounds that inhibited both pNP-TMP and FS-3 hydrolysis. The 26 compounds were next counter-screened in the presence of 0.01% Triton X-100 discarding 11 promiscuous aggregators (data not shown). Finally, the ability of the compounds at 10 μM to inhibit ADMAN-LPC hydrolysis with a hit cutoff at 50% was used as the concluding criterion (Figures 2B and 3C). Only compound ***3*** in the dual-inhibitor group and compounds ***1*** and ***2*** in the single-inhibitor group met these criteria and were further characterized in cell-based assays and *in vivo*. These three compounds were tested for the inhibition of the ATX-mediated hydrolysis of LPC 14:0, LPC 16:0, LPC 18:0, and LPC 18:1 (Table 1) and found to inhibit the cleavage of all four molecular species of the substrate with similar efficacy when applied at 10 μM.

Mechanism of inhibition of the hit compounds. The mechanism of inhibition of ATX activity by the three compounds was determined by measuring the K_i, and/or K_i' values against ATX-mediated hydrolysis of FS-3 and pNP-TMP (Table 2). These experiments indicated that all three compounds inhibit the hydrolysis of the LPL substrate FS-3 by a competitive mechanism. In addition, competition assays were conducted for compound ***3*** against pNP-TMP hydrolysis in which the compound was also found to act via competitive mechanism.

Molecular docking of the inhibitors into the ATX structure. The differences in substrate-specific inhibition by the two groups of compounds led us to hypothesize that they might interact with different surfaces of ATX, as has been suggested for other ATX inhibitors showing substrate-selective effects (Hoeglund et al, 2010b). Computational docking studies were performed using one of the recently solved crystal structures of ATX (2XR9, Figure 4). The crystallographic studies identified three hot spots in the ATX

Molecular Pharmacology Fast Forward. Published on June 21, 2013 as DOI: 10.1124/mol.113.087080
This article has not been copyedited and formatted. The final version may differ from this version.

structure (Figure 4A): 1) The catalytic site with Thr^{210} and the two Zn atoms, 2) A hydrophobic pocket, which accommodates the hydrocarbon tail of the lipid substrate and product, and 3) A hydrophobic channel that is hypothesized to provide entry to LPC and exit to LPA. The best docking poses obtained for compounds ***1*** and ***2*** show that these molecules are oriented similarly within the hydrophobic pocket (Figure 4 B and C). The aromatic moieties of these compounds were inserted deeply into the pocket. However, these compounds do not reach the catalytic site. In contrast, compound ***3*** fits near the Zn^{2+} atoms at the catalytic site, almost in complete overlap with the position occupied by the covalently bound inhibitor HA-155. The computed placement of compound ***3*** is consistent with the disruption of the catalysis of both LPL and PDE substrates just as shown experimentally (Figure 4D).

Comparison of the docked positions of compounds ***1*** and ***2*** predicted that they are within 4.5 Å of residues Ser^{170}, Phe^{211}, Leu^{214}, Ala^{218}, Phe^{274}, Phe^{275}, Ala^{305}, and Tyr^{307} , which were defined as a hydrophobic pocket that accommodates the lipid tail of the substrate in the crystal structure (Hausmann et al., 2011; Nishimasu et al., 2011). In contrast, compound ***3*** was anchored within the catalytic binding site indicated by a predicted interaction with residues near the Zn^{2+} atoms. *In silico* calculation of energies of interaction of residues lining the hydrophobic pocket with compounds ***1*** and ***2*** predict more robust contribution to binding energy compared to compound ***3*** (Table 3). Thus, results of our molecular docking suggest that interactions with residues of the hydrophobic pocket play a fundamental role in the ATX inhibitory activity of compounds ***1*** and ***2***.

Mutagenesis of hydrophobic residues predicted to interact with the single

Molecular Pharmacology Fast Forward. Published on June 21, 2013 as DOI: 10.1124/mol.113.087080
This article has not been copyedited and formatted. The final version may differ from this version.

inhibitor compounds. Although *in silico* predictions suggested Tyr^{307} and Phe^{211} have the strongest binding energy, when mutating these residues we encountered problems with lack of expression and/or activity of the ATX mutants (Supplemental Figure 2) as noted previously by Hausmann et al. (Hausmann et al., 2011; Nishimasu et al., 2011). From the dock simulation we hypothesized a possible amino-aromatic interaction of Phe^{275} with regions of the inhibitors.

Thus, Phe^{275} was selected as a target hydrophobic residue, while Tyr^{83} was selected as a target residue in the vicinity, but outside of the hydrophobic channel and the catalytic site (Figure 5). We hypothesize that these two mutants would have different sensitivity to the inhibitors. Specifically, the $Y^{83}A$, 10.28 Å away, should maintain wild type properties when challenged with any of the inhibitors, whereas the single inhibitors should be more affected by the $F^{275}A$ replacement (Figure 5). Replacement of Phe^{275} and Tyr^{83} with alanine proved to be successful by yielding an enzyme that was active cleaving LPL and PDE substrates (Supplemental Figure 2). Characterization of the $F^{275}A$ mutant showed a greater loss in inhibitory potency by compound ***1*** than that of compound ***3*** (Table 4). The inhibitory potency of compound ***2*** also decreased by three-fold. Furthermore, characterization of the $Y^{83}A$ mutant supported our hypothesis by revealing that this mutation had no significant impact on the effect of either type of inhibitor. The differential effect of the Phe^{275} mutation on the inhibitory potency of the single inhibitors lends support to the unique interactions these compounds have with the surface of the hydrophobic pocket.

Characterization of the ATX Inhibitors on Other Pharmacologically Relevant Targets. As a member of the NPP family of enzymes, ATX shares homology with NPP6

Molecular Pharmacology Fast Forward. Published on June 21, 2013 as DOI: 10.1124/mol.113.087080
This article has not been copyedited and formatted. The final version may differ from this version.

and NPP7, which are type C phospholipases. NPP6 cleaves phosphocholine from LPC, sphingosylphosphorylcholine and glycerophosphorylcholine (Sakagami et al., 2005). NPP7 hydrolyzes sphingomyelin to generate ceramide and can also cleave phosphocholine from LPC and platelet activating factor to generate monoacyl- and alkyl-acetyl glycerols (Duan et al., 2003; Wu et al., 2006). The selectivity of the ATX inhibitors was examined against NPP6 and NPP7. None of the inhibitors had a significant effect on NPP6/7-mediated hydrolysis of the synthetic substrate, *p*-nitrophenylphosphocholine.

In order to determine potential off-target effects that the three hit compounds may have we submitted them to the National Institute of Mental Health Psychoactive Drug Screening Program (http://pdsp.med.unc.edu/ indexR.html). The compounds were tested for modulation of 32 types and subtypes of GPCR including seven lysophospholipid receptors—including $S1P_{2/3/4/5}$ and $LPA_{1/2/3}$—16 orphan receptors, 6 transporters and three ion channels that included the HERG2 channel. The results of this extensive screen showed no activating or inhibitory action by compounds ***1*** and ***3*** on any of these targets up to 10 μM the highest concentration tested. We also extended the characterization of the three ATX inhibitors to the non-EDG family LPA receptors LPA_4 and LPA_5 and found no agonist, antagonist, or inhibitory action up to 10 μM, the highest concentration tested (data not shown).

Effect of the ATX inhibitors on A2058 melanoma cell invasion. ATX was originally discovered as a proinvasive factor in the culture supernatant of A2058 melanoma cells (Stracke et al., 1992). For this reason, we elected to evaluate the three new inhibitors on the invasion of this human melanoma cell line. We applied recombinant 0.3 nM ATX

Molecular Pharmacology Fast Forward. Published on June 21, 2013 as DOI: 10.1124/mol.113.087080
This article has not been copyedited and formatted. The final version may differ from this version.

plus 1μM of 18:1 LPC with or without increasing concentrations of the inhibitors and quantified the invasion of matrigel-coated BD BioCoat^{TM} chambers 16 h later. The dose response-curves generated (Figure 6A) showed comparable nanomolar IC_{50} regardless of the blocking site of the compound in ATX. Specifically, the IC_{50} values were 118.79 ± 62.9 nM, 153.05 ± 59.5 nM, and 85.35 ± 44.6 nM, for compounds ***1, 2***, and ***3,*** respectively.

Effect of the ATX inhibitors on B16-F10 melanoma cell metastasis. C57BL/6 mice injected with the syngeneic B16-F10 melanoma cells via the tail vein metastasize primarily to the lungs in an ATX-dependent manner (Baker et al., 2006; Gotoh et al., 2012; Gupte et al., 2011). We showed that in this model administration of an ATX inhibitor up to 48 h post-inoculation of the melanoma cells still causes a significant reduction in the number of metastatic lung nodules indicating a role for ATX in the colonization and seeding of the lungs with melanoma cells (Gotoh et al., 2012). We tested compound ***1*** and ***3*** by treating mice 1 day prior or 1 day after inoculation of B16-F10 melanoma cells via the tail vein, and continued for additional 10 days. We also included 4-pentadecyl benzylphosphonic acid, a previously validated ATX inhibitor in the pre- and post-inoculation paradigm (Gupte et al., 2011). The single inhibitor compound ***1*** caused a significant reduction in the number of lung nodules in both treatment paradigms (Figure 6B). The dual inhibitor compound ***3*** caused a significant reduction in the metastatic nodules in the pretreatment paradigm but it did not reach significance in the post-inoculation paradigm ($p = 0.056$). 4-Pentadecyl benzylphosphonic acid, which is also a dual-type inhibitor, caused a significant reduction in the number of metastatic nodules in the lungs (Gotoh et al., 2012; Gupte et al., 2010). Altogether, these findings

Molecular Pharmacology Fast Forward. Published on June 21, 2013 as DOI: 10.1124/mol.113.087080
This article has not been copyedited and formatted. The final version may differ from this version.

support the hypothesis that inhibition of ATX, regardless whether blocking the active site or the hydrophobic channel, small molecules can have similar blocking effects of melanoma metastasis *in vivo*.

Molecular Pharmacology Fast Forward. Published on June 21, 2013 as DOI: 10.1124/mol.113.087080
This article has not been copyedited and formatted. The final version may differ from this version.

Discussion

In this study we identified a surface of the hydrophobic pocket of ATX as a target site of inhibitors of enzymatic activity. The primary objective of the present study was to identify structurally diverse non-lipid inhibitors of ATX. We applied a HTS strategy using purified recombinant human β-ATX with the LPC-like substrate FS-3, which distinguishes our study from two previous HTS screens that utilized the PDE substrate pNP-TMP to screen a 13,000 member proprietary library with a partially purified mouse β-ATX from 3T3-F442A adipocytes (Ferry et al., 2008) or a 40,000 compound library using human recombinant ATX (Albers et al., 2010). Docking simulations of FS-3 into the ATX structure showed (Supplemental Figure 3) that the hydrocarbon chain of this substrate extends into the hydrophobic pocket, whereas the fluorochrome occupies a different space distinct from the hydrophobic channel of the enzyme. This model suggests that if one were to use pNP-TMP-like nucleotide substrates for HTS all compounds that bind to the hydrophobic pocket would be missed. Thus, our results favor the use of LPC-like substrates that engage both the active site and the hydrophobic pocket of ATX. Ferry et al. (Ferry et al., 2008) noted that in their hands ATX, once purified, precipitated, which led to them applying hexadecyl trimethylammonium bromide or 2-methyl-2,4-pentanediol detergent in their assays. These detergents did have an impact on the IC_{50} values they detected for their inhibitors. In our case the use of the human recombinant ATX did not present solubility problems, and the assay was linear up to 6 h, the latest point tested. Nonetheless, we also retested our hits in the presence of 0.01% Triton X-100, not because of the poor stability of the enzyme but rather to eliminate self-aggregating compounds leading to

Molecular Pharmacology Fast Forward. Published on June 21, 2013 as DOI: 10.1124/mol.113.087080
This article has not been copyedited and formatted. The final version may differ from this version.

false positives in the ATX inhibition assay (Feng et al., 2005). Our three-tiered assays (Figure 2 & Table 1) using LPC, PDE- and LPC-like substrates consistently identified several inhibitor hits against the different types of substrates. The ~10,000 compound diversity set was selected to be representative of the full compound library after application of a range of property and structural filters, affording a set of compounds significantly more drug-like and diverse. Chemoinformatics calculations and comparisons between compounds were performed within Pipeline Pilot (Pipeline Pilot Ver. 8.0.1.600, 2010 Accelrys Software Inc.). The UC Compound Library was evaluated according to the popular property filters (Hann and Oprea, 2004; Lipinski et al., 2001; Veber et al., 2002) targeting improved oral bioavailability or starting points for optimization toward improved oral bioavailability (i.e. fragment or lead-like), and from this evaluation the diversity set was compiled. The 9,652 compound diversity set we used is adherent to 3 out of 4 Lipinski Rules (Lipinski et al., 2001) drug-like property constraints.

Even though the hit rate in the primary screen was only ~2% using the 10 μM concentration and 50% inhibition criterion, the HTS identified 198 structurally diverse non-lipid inhibitor compounds. These compounds fall into multiple structural categories, and we have already noticed that some structural features such as presence of an aromatic sulfonamide group shows up in a disproportionately high number of the initial hits. This list of hits is now being used for the development of a structure based ATX inhibitor pharmacophore and will be discussed in a future report.

Tests conducted using pNP-TMP and the LPC-like substrates distinguished two groups of compounds. The first group inhibited the LPL activity against different naturally

Molecular Pharmacology Fast Forward. Published on June 21, 2013 as DOI: 10.1124/mol.113.087080
This article has not been copyedited and formatted. The final version may differ from this version.

occurring LPC species (Table **1**) and LPC-like substrates that included FS-3 and ADMAN-LPC (Figure 3C). In contrast, the second type of compounds inhibited both pNP-TMP and the LPL substrates. The mechanism of inhibition, regardless of the type of substrate, for both types of compounds was consistent with the results of computational docking. Nishimasu and colleagues (Nishimasu et al., 2012) proposed three important molecular interaction surfaces in ATX (Figure 4A). These included the active site, a hydrophobic pocket harboring the lipid tail, and a channel through which the substrate and the product can shuttle in-and-out from the active site. Our docking simulations place the dual inhibitor compound ***3*** in the vicinity of the active site overlapping with the space occupied by the covalent inhibitor HA-155 in the crystal structure (Figures 3D and 4D). The docked position of compound ***3*** provides a rational explanation for the inhibition of both types of substrates by blocking their interaction with the active site. In contrast, compounds ***1 and 2*** docked into the hydrophobic pocket sufficiently far away from the active site allowing for the hypothesis that these inhibitors selectively block the hydrolysis of lipid substrates (Figure 5E and 5F).

The hydrophobic pocket of ATX is lined by residues Ile^{168}, Phe^{211}, Leu^{217}, Ala^{218}, Leu^{260}, Phe^{274}, Phe^{275}, Trp^{261}, and Met^{513} [all human ATX residue numbers, (Nishimasu et al., 2011)] (Figure 6). Based on our docking simulation, Phe^{275} has an amino-aromatic interaction with compound ***1*.** This is demonstrated by the strong effect of the Phe^{275} mutant on the potency of compound ***1*** and the absence of effect on the potency of compound ***3***. Analysis of the $F^{275}A$ mutant ATX showed that it retained nearly wild type catalytic activity toward FS-3 and pNP-TMP substrates for compound ***3***. However, it lost its inhibition by compound ***1***, and its inhibition by compound ***2*** was also diminished

Molecular Pharmacology Fast Forward. Published on June 21, 2013 as DOI: 10.1124/mol.113.087080
This article has not been copyedited and formatted. The final version may differ from this version.

(Table 4).

The hits we identified in the DDC library have fulfilled one of our objectives for compounds that are non-lipid with partition coefficients in the range 2.99 and 3.98 that make them more water soluble than previously identified lipid-like inhibitors with logP values greater than 5 (Albers and Ovaa, 2012). Interestingly, the two single inhibitors had lower logP values than the dual inhibitor compound ***3***. This observation suggests that compounds with reasonable water solubility can access the hydrophobic binding pocket of ATX.

We had compound ***1*** and ***3*** tested for off target effects using the Psychoactive Drug Screening Program provided by the National Institutes of Mental Health. This extensive screen turned up no activity of these compounds at the thirty plus GPCRs, ion channels, and transporter targets that included the $S1P_2$, $S1P_3$, $S1P_4$, and $S1P_5$ sphingosine-1-phosphate GPCRs, the LPA_1, LPA_2, and LPA_3 LPA receptors, and the HERG-2 channel. The lack of agonist or antagonist action of our new ATX inhibitors on LPA and sphingosine-1-phosphate receptors combined with their lack of inhibitory activity at NPP6 and NPP7 underlines the specificity of these compounds to ATX and paves the way toward their use in cell-based and *in vivo* disease models.

The solubility, stability, and hence the bioavailability of several earlier ATX inhibitors have presented problems for their further development (Albers et al., 2010; Albers and Ovaa, 2012; Ferry et al., 2008). ATX was originally isolated as a factor that promoted melanoma invasion (Stracke et al., 1992) To assess the utility of the two types of inhibitors we tested their ability to inhibit invasion in a Boyden chamber cell-based assay. and our findings with both types of inhibitors confirmed that blocking the enzyme

Molecular Pharmacology Fast Forward. Published on June 21, 2013 as DOI: 10.1124/mol.113.087080
This article has not been copyedited and formatted. The final version may differ from this version.

inhibits the invasion of A2058 melanoma cells. At this early stage of the characterization of these novel ATX inhibitors we deemed it premature to conduct pharmacokinetic studies, however, we tested compounds ***1*** and ***3*** in the lung colonization model using B16-F10 syngeneic melanoma cells. These results indicated that the hydrophobic pocket inhibitor compound ***1*** was effective in significantly reducing the number of lung metastases when applied 1 day prior or 1 day after the inoculation with the tumor cells. This observation extends our previous reports that inhibition of ATX reduces the seeding of lung metastases in this animal model. This is the first set of results that shows the anti-metastatic utility of a compound that blocks the hydrophobic pocket without interfering with the PDE activity of the enzyme. It is in line with the previous hypothesis that the PDE activity of ATX does not play a role in the prometastatic action of this enzyme *in vivo*.

The present results taken together establish the utility of the compounds ***1*** and ***2*** for *in vitro* studies. Nonetheless, we view these compounds as primary hits that will have to undergo lead optimization to reach broad applicability *in vivo*.

Molecular Pharmacology Fast Forward. Published on June 21, 2013 as DOI: 10.1124/mol.113.087080
This article has not been copyedited and formatted. The final version may differ from this version.

Acknowledgements

Human receptor profiling and K_i data were generously provided by the National Institute of Mental Health's Psychoactive Drug Screening Program (NIMH PDSP). The NIMH PDSP is directed by B. Roth MD, PhD at the University of North Carolina at Chapel Hill and Project Officer J. Driscol at NIMH, Bethesda MD, USA. Contract # NO1MH32004.

Molecular Pharmacology Fast Forward. Published on June 21, 2013 as DOI: 10.1124/mol.113.087080
This article has not been copyedited and formatted. The final version may differ from this version.

Authorship Contributions

Participated in research design: Fells, Lee, Fujiwara, Norman, Tsukahara, Patil, Kirby, Nelson, Parrill, Miller, Tigyi.

Conducted experiments: Fells, Lim, Liu, Lee, Fujiwara, Norman, Tsukahara*, Patil, Kirby, Nelson.*

Contributed new reagents or analytic tools: Fells, Norman, Tsukahara*, Patil, Kirby, Nelson,* Seibel*,* Papoian*, Bittman, Baker.*

Performed data analysis: Fells, Lee, Fujiwara, Lim, Norman, Kirby, Nelson, Seibel*, Parrill, Tigyi.*

Wrote or contributed to the writing of the manuscript: Fells, Lee, Fujiwara, Norman, Parrill, Baker, Tigyi.

Molecular Pharmacology Fast Forward. Published on June 21, 2013 as DOI: 10.1124/mol.113.087080
This article has not been copyedited and formatted. The final version may differ from this version.

References

Albers HM, Dong A, van Meeteren LA, Egan DA, Sunkara M, van Tilburg EW, Schuurman K, van Tellingen O, Morris AJ, Smyth SS, Moolenaar WH and Ovaa H (2010) Boronic acid-based inhibitor of autotaxin reveals rapid turnover of LPA in the circulation. *Proc Natl Acad Sci U S A* **107**(16):7257-7262.

Albers HM and Ovaa H (2012) Chemical evolution of autotaxin inhibitors. *Chem Rev* **112**(5):2593-2603.

Baker DL, Fujiwara Y, Pigg KR, Tsukahara R, Kobayashi S, Murofushi H, Uchiyama A, Murakami-Murofushi K, Koh E, Bandle RW, Byun HS, Bittman R, Fan D, Murph M, Mills GB and Tigyi G (2006) Carba analogs of cyclic phosphatidic acid are selective inhibitors of autotaxin and cancer cell invasion and metastasis. *J Biol Chem* **281**(32):22786-22793.

Brindley DN, Lin FT and Tigyi GJ (2013) Role of the autotaxin-lysophosphatidate axis in cancer resistance to chemotherapy and radiotherapy. *Biochim Biophys Acta* **1831**(1):74-85.

Chemical Computing Group Inc. (2012) Molecular Operating Environment (MOE).

Clair T, Aoki J, Koh E, Bandle RW, Nam SW, Ptaszynska MM, Mills GB, Schiffmann E, Liotta LA and Stracke ML (2003) Autotaxin hydrolyzes sphingosylphosphorylcholine to produce the regulator of migration, sphingosine-1-phosphate. *Cancer Res* **63**(17):5446-5453.

David M, Wannecq E, Descotes F, Jansen S, Deux B, Ribeiro J, Serre CM, Gres S, Bendriss-Vermare N, Bollen M, Saez S, Aoki J, Saulnier-Blache JS, Clezardin P and Peyruchaud O (2010) Cancer cell expression of autotaxin controls bone metastasis formation in mouse through lysophosphatidic acid-dependent activation of osteoclasts. *PLoS One* **5**(3):e9741.

Duan RD, Bergman T, Xu N, Wu J, Cheng Y, Duan J, Nelander S, Palmberg C and Nilsson A (2003) Identification of human intestinal alkaline sphingomyelinase as a novel ecto-enzyme related to the nucleotide phosphodiesterase family. *J Biol Chem* **278**(40):38528-38536.

Feng BY, Shelat A, Doman TN, Guy RK and Shoichet BK (2005) High-throughput assays for promiscuous inhibitors. *Nat Chem Biol* **1**(3):146-148.

Ferry G, Moulharat N, Pradere JP, Desos P, Try A, Genton A, Giganti A, Beucher-Gaudin M, Lonchampt M, Bertrand M, Saulnier-Blache JS, Tucker GC, Cordi A and Boutin JA (2008) S32826, a nanomolar inhibitor of autotaxin: discovery, synthesis and applications as a pharmacological tool. *J Pharmacol Exp Ther* **327**(3):809-819.

Forli S (2013) Raccoon|AutoDock VS: an automated tool for preparing AutoDock virtual screenings http://autodock.scripps.edu/resources/raccoon.

Gierse J, Thorarensen A, Beltey K, Bradshaw-Pierce E, Cortes-Burgos L, Hall T, Johnston A, Murphy M, Nemirovskiy O, Ogawa S, Pegg L, Pelc M, Prinsen M, Schnute M, Wendling J, Wene S, Weinberg R, Wittwer A, Zweifel B and Masferrer J (2010) A novel autotaxin inhibitor reduces lysophosphatidic acid levels in plasma and the site of inflammation. *J Pharmacol Exp Ther* **334**(1):310-317.

Gijsbers R, Aoki J, Arai H and Bollen M (2003) The hydrolysis of lysophospholipids and

nucleotides by autotaxin (NPP2) involves a single catalytic site. *FEBS Lett* **538**(1-3):60-64.

Gotoh M, Fujiwara Y, Yue J, Liu J, Lee S, Fells J, Uchiyama A, Murakami-Murofushi K, Kennel S, Wall J, Patil R, Gupte R, Balazs L, Miller DD and Tigyi GJ (2012) Controlling cancer through the autotaxin-lysophosphatidic acid receptor axis. *Biochem Soc Trans* **40**(1):31-36.

Gupte R, Patil R, Liu J, Wang Y, Lee SC, Fujiwara Y, Fells J, Bolen AL, Emmons-Thompson K, Yates CR, Siddam A, Panupinthu N, Pham TC, Baker DL, Parrill AL, Mills GB, Tigyi G and Miller DD (2011) Benzyl and Naphthalene Methylphosphonic Acid Inhibitors of Autotaxin with Anti-invasive and Anti-metastatic Activity. *Chem Med Chem* **6**(5):922-935.

Gupte R, Siddam A, Lu Y, Li W, Fujiwara Y, Panupinthu N, Pham TC, Baker DL, Parrill AL, Gotoh M, Murakami-Murofushi K, Kobayashi S, Mills GB, Tigyi G and Miller DD (2010) Synthesis and pharmacological evaluation of the stereoisomers of 3-carba cyclic-phosphatidic acid. *Bioorg Med Chem Lett* **20**(24):7525-7528.

Hann M and Oprea T (2004) Pursuing the leadlikeness concept in pharmaceutical research. . *Cur Opinion in Chem Biol* **8**(3):255-263.

Hausmann J, Kamtekar S, Christodoulou E, Day JE, Wu T, Fulkerson Z, Albers HM, van Meeteren LA, Houben AJ, van Zeijl L, Jansen S, Andries M, Hall T, Pegg LE, Benson TE, Kasiem M, Harlos K, Kooi CW, Smyth SS, Ovaa H, Bollen M, Morris AJ, Moolenaar WH and Perrakis A (2011) Structural basis of substrate discrimination and integrin binding by autotaxin. *Nat Struct Mol Biol* **18**(2):198-204.

Hoeglund AB, Bostic HE, Howard AL, Wanjala IW, Best MD, Baker DL and Parrill AL (2010) Optimization of a pipemidic acid autotaxin inhibitor. *J Med Chem* **53**(3):1056-1066.

Houben AJ and Moolenaar WH (2011) Autotaxin and LPA receptor signaling in cancer. *Cancer Metastasis Rev* **30**(3-4):557-565.

Ikeda H and Yatomi Y (2012) Autotaxin in liver fibrosis. *Clin Chim Acta* **413**(23-24):1817-1821.

Kawaguchi M, Okabe T, Okudaira S, Nishimasu H, Ishitani R, Kojima H, Nureki O, Aoki J and Nagano T (2013) Screening and X-Ray Crystal Structure-based Optimization of Autotaxin (ENPP2) Inhibitors, Using a Newly Developed Fluorescence Probe. *ACS Chem Biol*.

Kehlen A, Englert N, Seifert A, Klonisch T, Dralle H, Langner J and Hoang-Vu C (2004) Expression, regulation and function of autotaxin in thyroid carcinomas. *Int J Cancer* **109**(6):833-838.

Koh E, Clair T, Woodhouse EC, Schiffmann E, Liotta L and Stracke M (2003) Site-directed mutations in the tumor-associated cytokine, autotaxin, eliminate nucleotide phosphodiesterase, lysophospholipase D, and motogenic activities. *Cancer Res* **63**(9):2042-2045.

Kremer AE, van Dijk R, Leckie P, Schaap FG, Kuiper EM, Mettang T, Reiners KS, Raap U, van Buuren HR, van Erpecum KJ, Davies NA, Rust C, Engert A, Jalan R, Oude Elferink RP and Beuers U (2012) Serum autotaxin is increased in pruritus of cholestasis, but not of other origin, and responds to therapeutic interventions. *Hepatology* **56**(4):1391-1400.

Lipinski C, Lombardo F, Dominy B and Feeney P (2001) Experimental and computational approaches to estimate solubility and permeability in drug discovery and development settings. *Adv Drug Del Rev* **46**:3-26.

Mills GB and Moolenaar WH (2003) The emerging role of lysophosphatidic acid in cancer. *Nat Rev Cancer* **3**(8):582-591.

Mize CD, Abbott AM, Gacasan SB, Parrill AL and Baker DL (2011) Ligand-based autotaxin pharmacophore models reflect structure-based docking results. *J Mol Graph Model* **31**:76-86.

Moolenaar WH, Houben AJ, Lee SJ and van Meeteren LA (2013) Autotaxin in embryonic development. *Biochim Biophys Acta* **1831**(1):13-19.

Nikitopoulou I, Oikonomou N, Karouzakis E, Sevastou I, Nikolaidou-Katsaridou N, Zhao Z, Mersinias V, Armaka M, Xu Y, Masu M, Mills GB, Gay S, Kollias G and Aidinis V (2012) Autotaxin expression from synovial fibroblasts is essential for the pathogenesis of modeled arthritis. *J Exp Med* **209**(5):925-933.

Nishimasu H, Ishitani R, Aoki J and Nureki O (2012) A 3D view of autotaxin. *Trends Pharmacol Sci* **33**(3):138-145.

Nishimasu H, Okudaira S, Hama K, Mihara E, Dohmae N, Inoue A, Ishitani R, Takagi J, Aoki J and Nureki O (2011) Crystal structure of autotaxin and insight into GPCR activation by lipid mediators. *Nat Struct Mol Biol* **18**(2):205-212.

North EJ, Howard AL, Wanjala IW, Pham TC, Baker DL and Parrill AL (2010) Pharmacophore development and application toward the identification of novel, small-molecule autotaxin inhibitors. *J Med Chem* **53**(8):3095-3105.

Nouh MA, Wu XX, Okazoe H, Tsunemori H, Haba R, Abou-Zeid AM, Saleem MD, Inui M, Sugimoto M, Aoki J and Kakehi Y (2009) Expression of autotaxin and acylglycerol kinase in prostate cancer: association with cancer development and progression. *Cancer Sci* **100**(9):1631-1638.

Sakagami H, Aoki J, Natori Y, Nishikawa K, Kakehi Y and Arai H (2005) Biochemical and molecular characterization of a novel choline-specific glycerophosphodiester phosphodiesterase belonging to the nucleotide pyrophosphatase/phosphodiesterase family. *J Biol Chem* **280**(24):23084-23093.

Saunders LP, Ouellette A, Bandle R, Chang WC, Zhou H, Misra RN, De La Cruz EM and Braddock DT (2008) Identification of small-molecule inhibitors of autotaxin that inhibit melanoma cell migration and invasion. *Mol Cancer Ther* **7**(10):3352-3362.

Schneider CA, Rasband WS and Eliceiri KW (2012) NIH Image to ImageJ: 25 years of image analysis. *Nat Methods* **9**(7):671-675.

St-Coeur PD, Ferguson D, Morin P, Jr. and Touaibia M (2013) PF-8380 and closely related analogs: synthesis and structure-activity relationship towards autotaxin inhibition and glioma cell viability. *Arch Pharm (Weinheim)* **346**(2):91-97.

Stracke ML, Krutzsch HC, Unsworth EJ, Arestad A, Cioce V, Schiffmann E and Liotta LA (1992) Identification, purification, and partial sequence analysis of autotaxin, a novel motility-stimulating protein. *J Biol Chem* **267**(4):2524-2529.

Tager AM (2012) Autotaxin emerges as a therapeutic target for idiopathic pulmonary fibrosis: limiting fibrosis by limiting lysophosphatidic acid synthesis. *Am J Resp Cell Mol Biol* **47**(5):563-565.

Tigyi G (2010) Aiming drug discovery at lysophosphatidic acid targets. *Br J Pharmacol*

161(2):241-270.

Trott O and Olson AJ (2010) AutoDock Vina: improving the speed and accuracy of docking with a new scoring function, efficient optimization, and multithreading. *J Comput Chem* **31**(2):455-461.

Ueda H, Matsunaga H, Olaposi OI and Nagai J (2013) Lysophosphatidic acid: Chemical signature of neuropathic pain. *Biochim Biophys Acta* **1831**(1):61-73.

Veber D, Johnson S, Cheng H-Y, Smith S, Ward K and Kopple K (2002) Molecular Properties That Influence the Oral Bioavailability of Drug Candidates. *J Med Chem* **45**(12):2615–2623.

Wu J, Nilsson A, Jonsson BA, Stenstad H, Agace W, Cheng Y and Duan RD (2006) Intestinal alkaline sphingomyelinase hydrolyses and inactivates platelet-activating factor by a phospholipase C activity. *Biochem J* **394**(Pt 1):299-308.

Wu JM, Xu Y, Skill NJ, Sheng H, Zhao Z, Yu M, Saxena R and Maluccio MA (2010) Autotaxin expression and its connection with the TNF-alpha-NF-kappaB axis in human hepatocellular carcinoma. *Mol Cancer* **9**:71.

Yanagida K, Kurikawa Y, Shimizu T and Ishii S (2013) Current progress in non-Edg family LPA receptor research. *Biochim Biophys Acta* **1831**(1):33-41.

Yang SY, Lee J, Park CG, Kim S, Hong S, Chung HC, Min SK, Han JW, Lee HW and Lee HY (2002) Expression of autotaxin (NPP-2) is closely linked to invasiveness of breast cancer cells. *Clin Exp Metastasis* **19**(7):603-608.

Yang Y, Mou L, Liu N and Tsao MS (1999) Autotaxin expression in non-small-cell lung cancer. *Am J Respir Cell Mol Biol* **21**(2):216-222.

Footnotes

This study was supported by National Institutes of Health National Cancer Institute [Grant CA092160]; the American Cancer S;ociety [Grant 122059-PF-12-107-01-CDD] and the Van Vleet Endowment.

Legends for figures:

Figure 1

Chemical structure of ATX inhibitors identified in the present study and HA155.

Figure 2

Schematic of enzyme reactions used for measuring ATX activity. A) FS-3 substrate used for high-throughput screening and in the counterscreen in the presence of 0.01% Triton X-100. B) pNP-TMP substrate used to for nucleotide hydrolysis by ATX. C) AD-MAN-LPC, a synthetic, fluorescent LPC analog to monitor ATX-catalyzed hydrolysis of LPC.

Figure 3

Identification and characterization of ATX inhibitors by high-throughput screening.

A. Dose-response curve of three most potent hits from the HTS.

B. Comparison of substrate selectivity against FS3 (filled bars) and pNP-TMP (open bars) for the three inhibitors applied at 10 μM. The inhibition was normalized to the cleavage of the substrate in the absence of the inhibitors designated as 100%.

C. Inhibition of ATX-mediated hydrolysis of ADMAN-LPC by inhibitors. A representative TLC image shows that ATX inhibitors applied at 10 μM inhibited the hydrolysis of 30 μM ADMAN-LPC by 30 nM ATX.

Figure 4

Molecular surfaces involved in catalysis, substrate binding and substrate/product access in ATX. A. This panel shows the three binding surfaces in the cocrystal of HA-155 in ATX. The catalytic center surface with the two Zn^{2+} ions is marked by the blue dotted line. The hydrophobic channel proposed to shuttle the substrate and the product

Molecular Pharmacology Fast Forward. Published on June 21, 2013 as DOI: 10.1124/mol.113.087080
This article has not been copyedited and formatted. The final version may differ from this version.

in and out from the catalytic site is marked with black dashed line. The hydrophobic pocket surface is delineated in purple dotted-dashed line. B. C. and D. show the energy minimized docked positions calculated by MOE (Chemical Computing Group Inc., 2012) for compounds ***1, 2,*** and ***3***, respectively. The orientation of the enzyme is the same in all panels. Panels E and F show pNP-TMP docked to the complexes of ATX with compound ***1*** and compound ***2***, respectively. Note the complete separation of this docked position of pNP-TMP and the two inhibitors. These models explain the lack of inhibition of pNP-TMP hydrolysis by compounds ***1*** and ***2*.**

Figure 5

Landmark residues (sticks) lining the hydrophobic pocket based on the ATX crystal structure. Docked substrate and inhibitors are shown in ball and stick models. A. LPC 18:1 substrate, B. Compound ***1***, C. Compound ***2***, and D. Compound ***3*** docked and energy minimized using the MOE software (Version 2009.10). In panels B-C the HA-155 inhibitor-bound crystal structure is overlayed in white. Phe^{275} is shown for reference in all panels. Note the close proximity of Phe^{275} to docked compounds ***1*** and ***2*** and the relatively large distance to compound ***3***.

Figure 6

Effects of ATX inhibitor hits on cancer cell invasion (A) and lung metastasis (B). A) A2058 human melanoma cells were applied to matrigel-coated BD BioCoat™ chambers. 0.3 nM ATX plus 1 μM of 18:1 LPC with or without increasing concentrations of the inhibitors was applied and invasion was quantified 16 h later. Note that all three compounds showed a dose-dependent inhibition of A2058 melanoma invasion.
B) C57BL/6 mice were inoculated with 7.5 x 10^4 B16-F10 melanoma cells via the tail

Molecular Pharmacology Fast Forward. Published on June 21, 2013 as DOI: 10.1124/mol.113.087080
This article has not been copyedited and formatted. The final version may differ from this version.

vein. Treatment with either compound ***1*****,** compound ***3*****,** or 4-pentadecylbenzylphosphonic acid (positive control) at 30 µg per mouse via intraperitoneal injection was started one day before (pretreatment) or after (posttreatment) the B16-F10 inoculation, and daily for an additional 10 days. Control mice were injected with vehicle (PBS with 10% PEG vehicle). The mice were sacrificed on postinoculation day 21 and the lung nodules were counted. P values were calculated using Student's t-test relative to the vehicle group.

Molecular Pharmacology Fast Forward. Published on June 21, 2013 as DOI: 10.1124/mol.113.087080
This article has not been copyedited and formatted. The final version may differ from this version.

Tables

Table 1. Inhibition of ATX-mediated Hydrolysis of Different LPC Species

	% Inhibition (± SD)			
	LPC 14:0	LPC 16:0	LPC 18:0	LPC 18:1
918013 (Compound ***1***)	41.0 ± 5.1	55.4 ± 1.7	43.6 ± 2.6	51.8 ± 2.4
931126 (Compound ***2***)	55.9 ± 0.5	69.0 ± 1.2	57.6 ± 0.9	61.9 ± 2.0
966791 (Compound ***3***)	70.3 ± 1.8	80.3 ± 1.0	78.2 ± 1.1	78.8 ± 0.7

ATX inhibition by the selected compounds was assessed via Amplex Red choline release assay. Fluorescence was read initially and after 2 hour incubation at 37°C at Ex/Em λ of 560/590 nm. Data (relative fluorescence) were then recorded as a mean value of the triplicates for each sample and reported as % inhibition of ATX-mediated LPC hydrolysis.

Molecular Pharmacology Fast Forward. Published on June 21, 2013 as DOI: 10.1124/mol.113.087080
This article has not been copyedited and formatted. The final version may differ from this version.

Table 2. Characterization of the hit compounds.

Compound	Partition Coefficient Log P	Assays and Result Type					
		FS-3			pNP-TMP		
		IC_{50} (nM)	Mechanism of Inhibition	Ki (nM)	IC_{50} (nM)	Mechanism of Inhibition	Ki (nM)
1	2.99	31.42	Competitive	12.98	N/A	N/A	N/A
2	3.54	6.50	Competitive	19.64	N/A	N/A	N/A
3	3.98	53.05	Competitive	7.14	314	Competitive	933

N/A – not applicable due lack of inhibition of pNP-TMP hydrolysis, IC_{50}- concentration that inhibits the cleavage of LPC by 50%, K_i – inhibitory constant,

Molecular Pharmacology Fast Forward. Published on June 21, 2013 as DOI: 10.1124/mol.113.087080
This article has not been copyedited and formatted. The final version may differ from this version.

Table 3. Modeled Energy of interactions (kJ/mol) and distances (Å) between selected ATX residues and inhibitors.

Residue	Compound ***1***		Compound ***2***		Compound ***3***	
	Energy	Distance	Energy	Distance	Energy	Distance
TYR^{307}	-14.51	1.78	-4.65	3.00	-3.12	1.49
PHE^{275}	-6.02	1.74	-8.67	1.66	-4.85	3.12
LEU^{214}	-3.74	3.87	-3.11	2.74	-0.36	4.29
PHE^{274}	-1.17	1.70	-2.17	2.88	NA	8.31
Thr^{210} (catalytic site)	NA	4.90	NA	6.79	-4.77	3.45
PHE^{211}	-1.07	2.40	-3.69	1.95	-30.55	2.62
ALA^{218}	-0.95	2.14	-0.08	1.66	NA	11.41
ALA^{305}	-0.92	2.82	-0.94	3.80	NA	9.74
SER^{170}	-0.34	2.26	-0.02	4.63	NA	7.60

Energy of interaction between individual residues and inhibitors calculated with Interaction Forces and Energies module of MOE for the optimized enzyme-inhibitor complexes. NA: not applicable because distance is > 4.5Å.

Molecular Pharmacology Fast Forward. Published on June 21, 2013 as DOI: 10.1124/mol.113.087080
This article has not been copyedited and formatted. The final version may differ from this version.

Table 4. Characterization of ATX mutants

	Compound *1*		**Compound *2***		**Compound *3***	
Substrate	FS-3	pNP-TMP	FS-3	pNP-TMP	FS-3	pNP-TMP
ATX Mutant	IC_{50} (μM)	IC_{50} (μM)	IC_{50} (μM)	IC_{50} (μM)	IC_{50} (μM)	IC_{50} (μM)
WT	3.0 ± 0.01	NE	0.13 ± 0.00	NE	0.41 ± 0.01	0.15 ± 0.01
$F^{275}A$	> 10.00	NE	0.32 ± 0.01	NE	2.5 ± 0.06	1.58 ± 0.05
$Y^{83}A$	0.15 ± 0.01	NE	0.06 ± 0.00	NE	0.19 ± 0.03	0.11 ± 0.01

NE: Compounds ***1 and 2*** had no effect on pNP-TMP hydrolysis

Molecular Pharmacology Fast Forward. Published on June 21, 2013 as DOI: 10.1124/mol.113.087080
This article has not been copyedited and formatted. The final version may differ from this version.

Figure 1

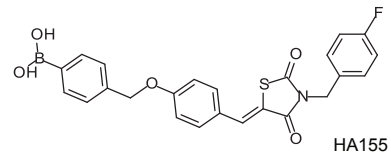

HA155

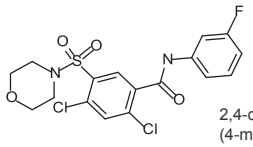

Compound **1**

2,4-dichloro-N-(3-fluorophenyl)-5-(4-morpholinylsulfonyl)benzamide

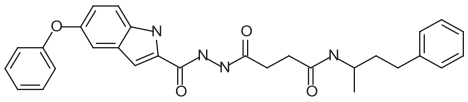

Compound **2**

1H-Indole-2-carboxylic acid, 5-phenoxy-, 2-[4-[(1-methyl-3-phenylpropyl)amino]-1,4-dioxobutyl] hydrazide

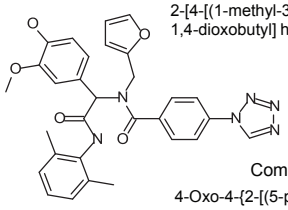

Compound **3**

4-Oxo-4-{2-[(5-phenoxy-1H-indol-2-yl)carbonyl]hydrazino}-N-(4-phenylbutan-2-yl)butanamide

Molecular Pharmacology Fast Forward. Published on June 21, 2013 as DOI: 10.1124/mol.113.087080
This article has not been copyedited and formatted. The final version may differ from this version.

Figure 2

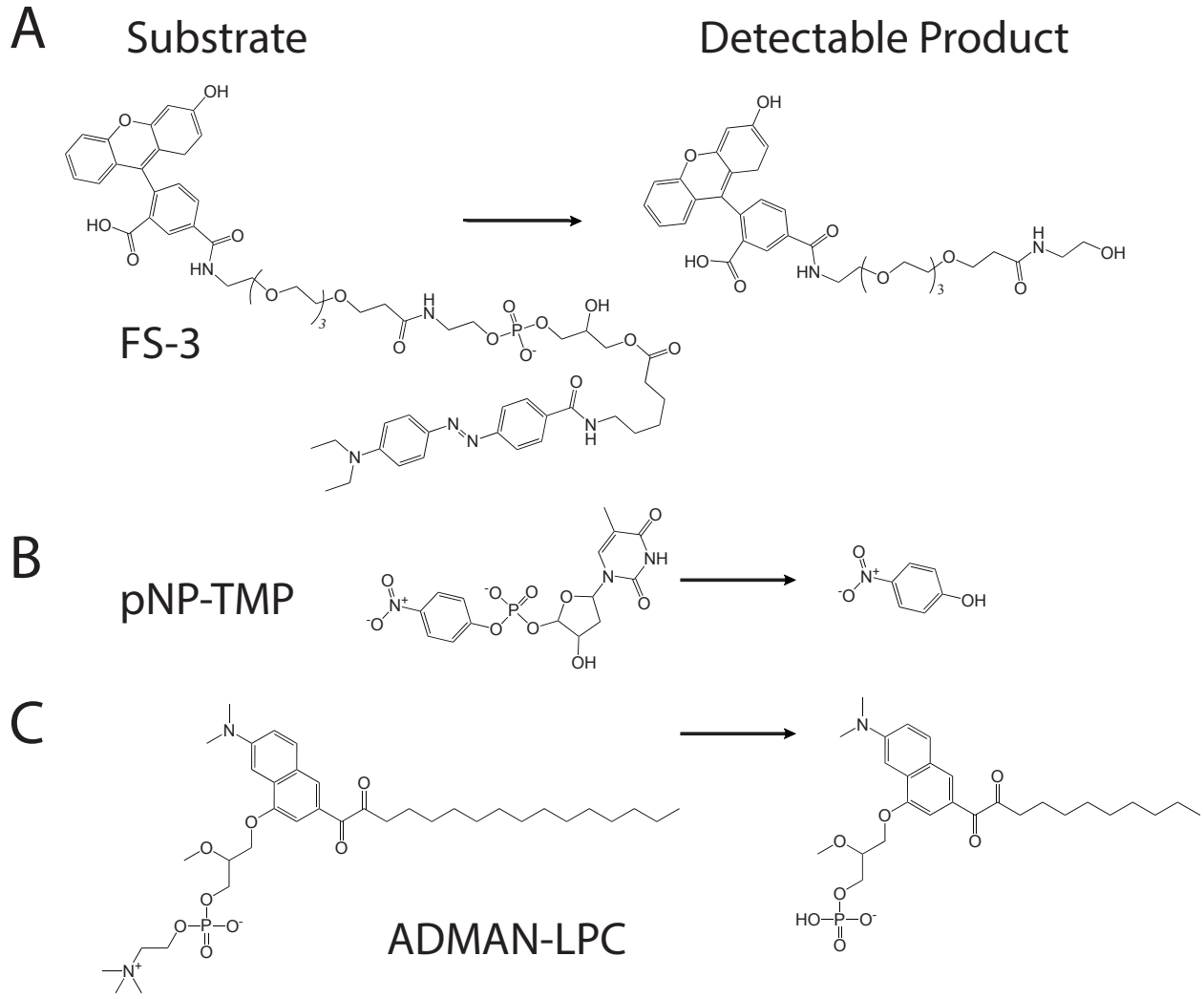

Figure 3 Molecular Pharmacology Fast Forward. Published on June 21, 2013 as DOI: 10.1124/mol.113.087080
This article has not been copyedited and formatted. The final version may differ from this version.

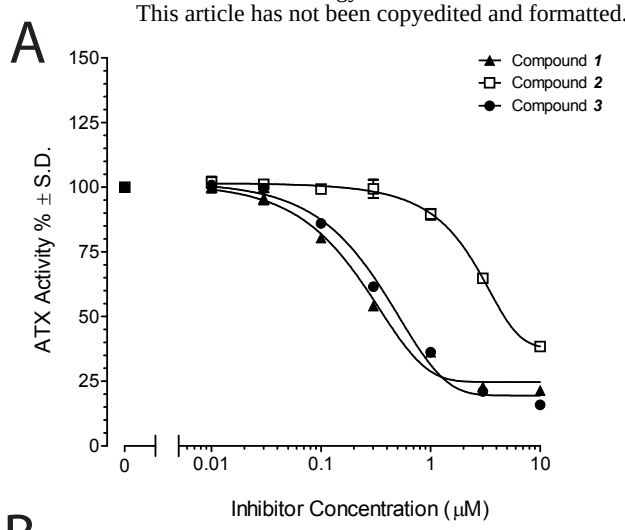

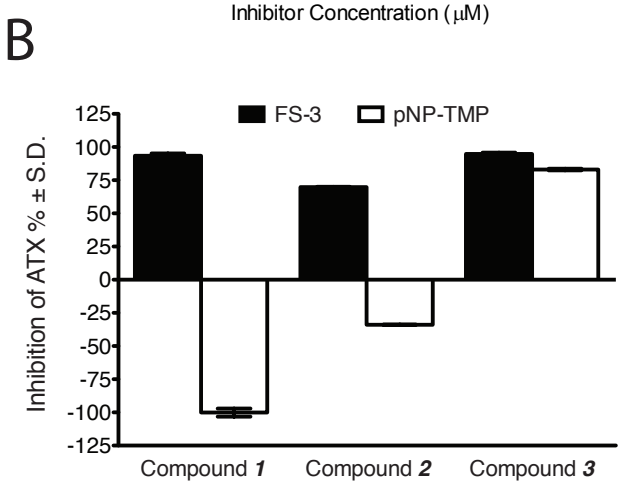

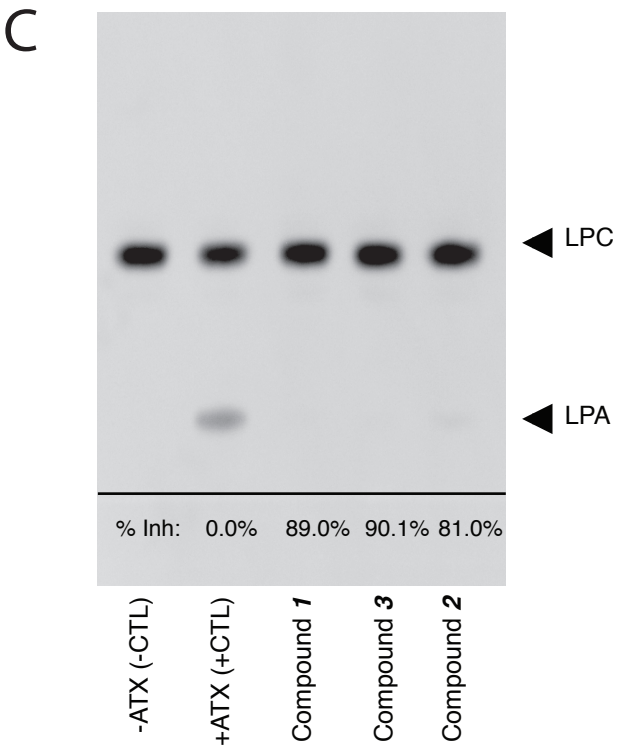

Molecular Pharmacology Fast Forward. Published on June 21, 2013 as DOI: 10.1124/mol.113.087080
This article has not been copyedited and formatted. The final version may differ from this version.

Figure 4

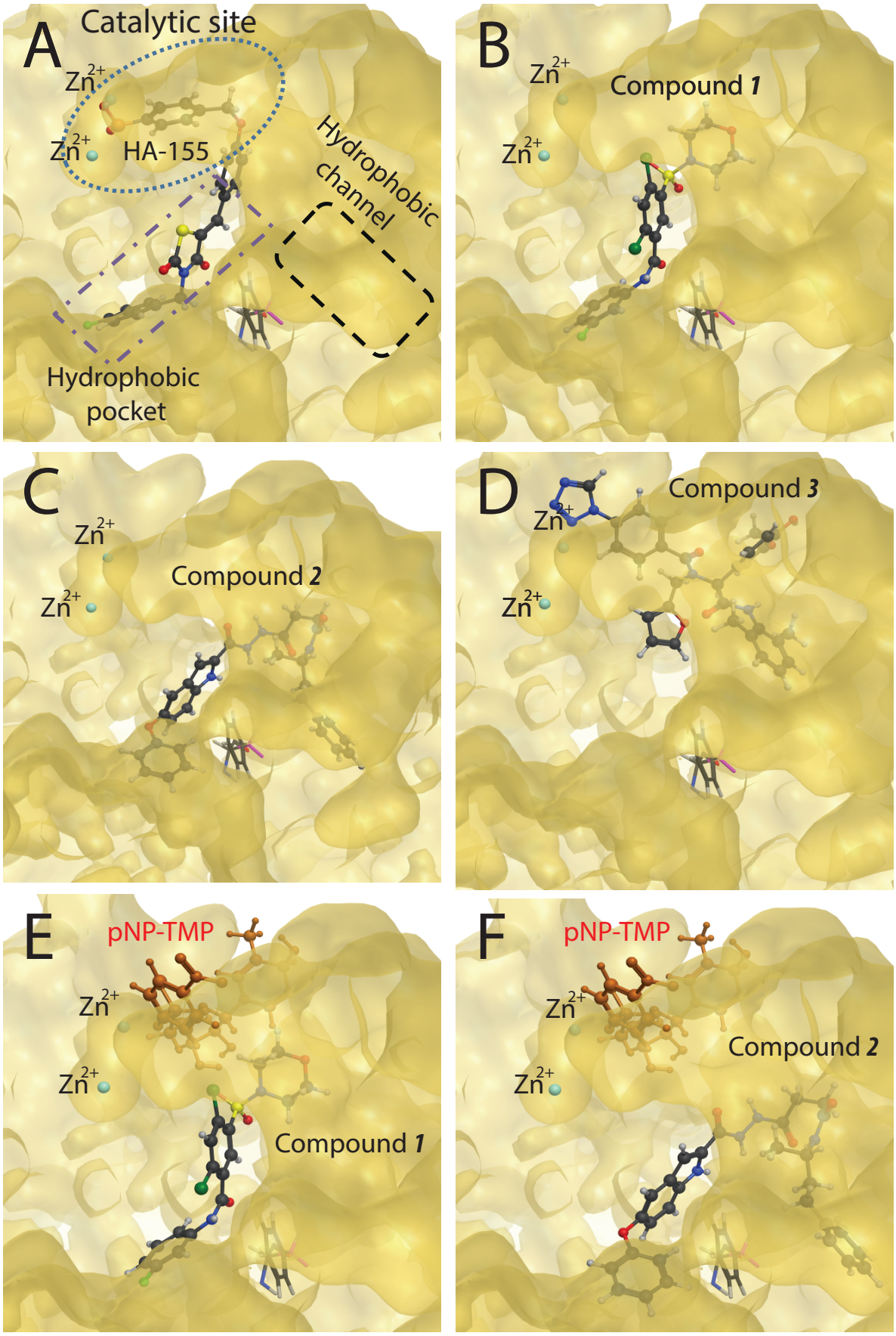

Molecular Pharmacology Fast Forward. Published on June 21, 2013 as DOI: 10.1124/mol.113.087080
This article has not been copyedited and formatted. The final version may differ from this version.

Figure 5

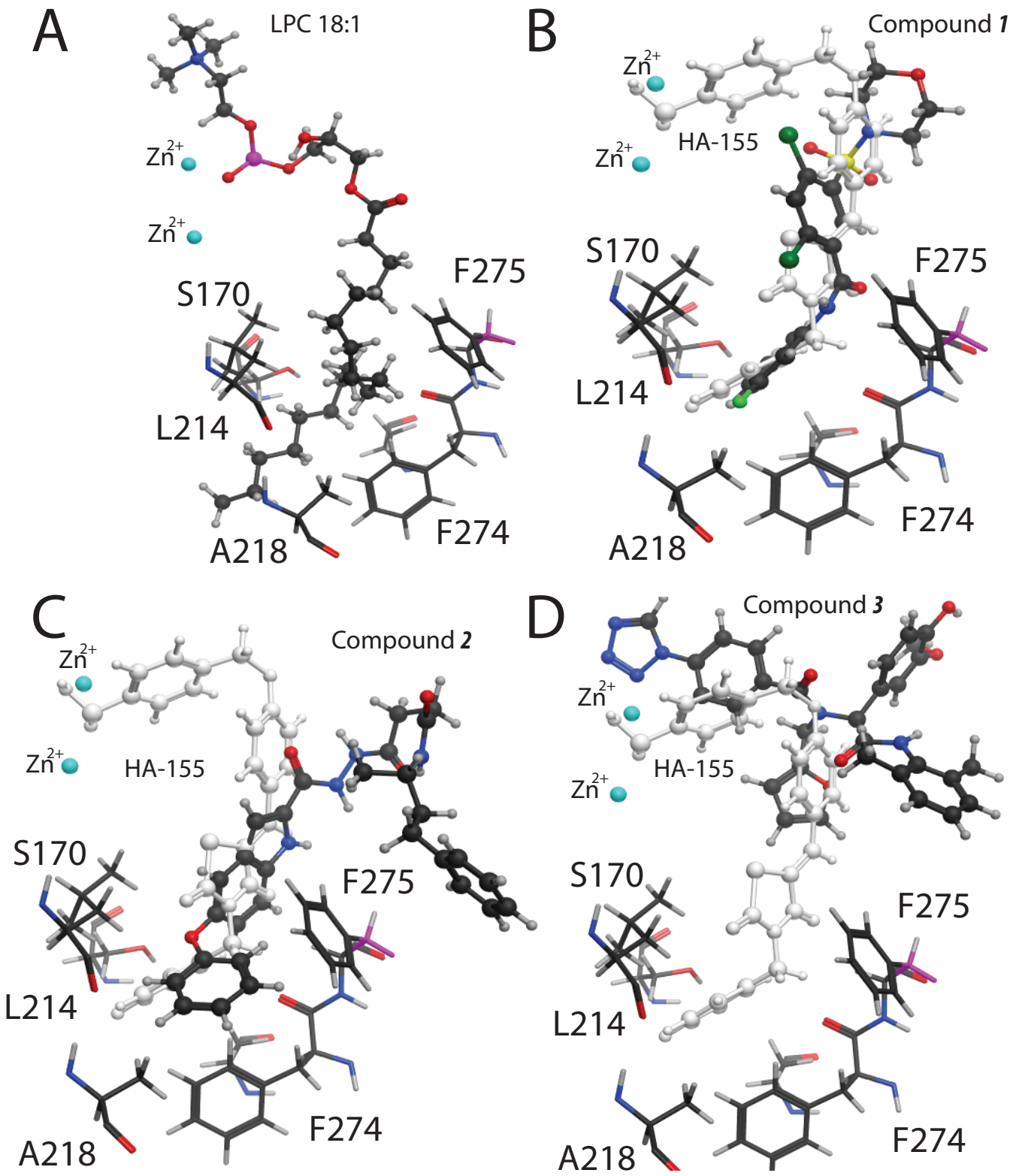

Molecular Pharmacology Fast Forward. Published on June 21, 2013 as DOI: 10.1124/mol.113.087080
This article has not been copyedited and formatted. The final version may differ from this version.

Figure 6